ACCEPTED VERSION

Iftekhair Ibnul Bashar, Alexander Bonaparte Sturm, Phillip Visintin and Abdul Hamid Sheikh
Analytical approach to quantify the pull-out behaviour of hooked end steel fibres
Australian Journal of Civil Engineering, 2024; 22(1):60-80

Analytical approach to quantify the pull-out behaviour of steel hooked fibre

Iftekhair Ibnul Bashar[1]; Alexander Bonaparte Sturm, Ph.D.[2]; Phillip Visintin, Ph.D.[3]; Abdul Hamid Sheikh, Ph.D.[4]

[1]Doctoral candidate, School of Civil, Environmental & Mining Engineering, The University of Adelaide SA5005 Australia. ORCID: https://orcid.org/0000-0002-3816-6431. Email: Iftekhair.bashar@adelaide.edu.au

[2]Assistant Professor, Department of Civil Engineering, National Cheng Kung University, Tainan City 701 Taiwan (R.O.C). ORCID: https://orcid.org/0000-0001-5881-5112. Email: asturm@gs.ncku.edu.tw

[3]Associate Professor, School of Civil, Environmental & Mining Engineering, The University of Adelaide SA5005 Australia. ORCID: https://orcid.org/0000-0002-4544-2043. Email: phillip.visintin@adelaide.edu.au

[4]Associate Professor, School of Civil, Environmental & Mining Engineering, The University of Adelaide SA5005 Australia (corresponding author). ORCID: https://orcid.org/0000-0002-2839-1707. Email: abdul.sheikh@adelaide.edu.au

Abstract: An analytical modelling approach is developed in this article to simulate the pull-out behaviour of a single straight/hooked fibre which is embedded in concrete matrix. The partial-interaction model is used to simulate the interfacial bond between the fibre and matrix along the entire fibre length throughout all stages of loading where additional axial and frictional forces due to straightening a hook is incorporated by simulating it as plastic hinges at the apex of bends. The analytical model is presented in a concise matrix form which helps to minimise the number of solution steps for the involved individual cases and provides a monolithic simplified implementation. A significant advantage of the approach is that it does not require fitting of a smoothing polynomial to show the full-range of fibre load-slip behaviour as it simulates the forces for straightening the fibre as it pulls through a bend and directly couples this to the interfacial bond forces.

Keywords: Straight fibre; hooked fibre; pull-out response; analytical solution; numerical analysis.

Introduction

The addition of fibre to concrete to produce fibre reinforced concrete (FRC) or ultrahigh performance fibre reinforced concrete (UHPFRC) has drawn significant attention because of the potential to improve material strength and ductility. At the member level, fibre bridging improves flexural behaviour by increasing post-cracking stiffness (Stang and Aare 1992; Meda et al. 2012), reducing crack-widths (Stang and Aare 1992; Li et al. 1993), and delaying the failure in concrete softening regions (Schumacher 2006; Eid 2020). Similarly for non-flexural members, the fibres restrain shear-sliding leading to significantly improve of shear capacity that may minimise the use of transverse reinforcement (Barr 1987; Casanova and Rossi 1997; Noghabai 2000; Choi et al. 2007).

To realise the major benefits of FRC at the member level, significant research were conducted at the material level to investigate the effects of fibre material properties (Zheng and Feldman 1995; Cadoni et al. 2009; Yu et al. 2014; Akcay and Oszar 2019), fibre geometry (Soulioti et al. 2011; Wille and Naaman 2012; Rossi 2013; Simoes et al. 2017), and fibre volume fraction (Sukontasukkul 2004; Soulioti et al. 2011; Chu et al. 2018; Chu and Kwan 2019). This previous research has identified that the addition of hooks, corrugations or twists to smooth straight fibres can significantly increase pull-out loads and energies, which in turn improves member behaviour. Importantly, the array of fibre materials, geometries and volume fractions that can be added to concretes of all types and grades generates combinations too numerous to be investigated empirically. It is therefore important that mechanics simulations to be available to help identify and develop promising combinations of fibre and substrate properties which can then be the focus of further empirical study.

Among the earliest investigations on single fibre pull-out of straight smooth fibres are the works of Stang et al. (1990) and Naaman et al. (1991), which can be considered as the foundation of the majority of later approaches. In both these works a partial-interaction (PI) approach was used to define a governing differential equation that linked the load and slip of the fibre through the interfacial bond properties; with the major differentiation between works being the definition of the bond properties. While being essential in laying the foundation for future modelling approaches on both straight and hooked fibres, both the work of Stang et al. (1990) and Naaman et al. (1991) are themselves limited to straight fibres.

The earliest models to incorporate the benefit of the addition of hooks along the fibre length are based on modifications to Naaman's straight fibre model. For example, Alwan (1999) developed an analytical model for hooked fibres by adding a contribution to the force arising from the development and rotation of a plastic hinge at the apex of the hook. Importantly, in this approach, the pull-out process up to the complete interfacial debonding of the fibre was assumed to be identical for both straight and hooked fibres and therefore the impact of the hook is only assumed to occur after complete interfacial debonding. Abdallah and Rees (2019) extended Alwan's approach to accommodate multiple hooks and additionally replace the plastic hinge idealisation with an elastic-plastic idealisation to allow for partially formed hinges. A significant limitation of Alwan's approach, and those derived from it, is that in assuming that the plastic behaviour at the hinges occurs only after complete interfacial debonding, it is not possible to model the interaction between the interfacial debonding and plastic hinge rotation. It is therefore necessary to fit a high order smoothing polynomial to produce continuous load-slip results that approximate empirical observations.

Other similar PI approaches have been developed by Cunha et al. (2010) and Soetens et al. (2013). In the work of Cunha et al. (2010) a hooked fibre was idealised as an equivalent straight

77 fibre to which an additional force was added to allow for the contribution of the hinges as a
78 function of the end-slip of the fibre. As a result of this idealisation, the relationship between
79 the slip and hinge force can only be determined empirically by subtracting the experimentally
80 observed behaviour of a straight fibre from the experimentally observed behaviour of a hooked
81 fibre. Soetens et al. (2013) presented a finite differences solution based on the PI model of
82 Stang et al. (1990), which assumed the fibre material to be rigid plastic. Friction after complete
83 de-bonding was determined empirically as a function of compressive strength and the model
84 further allowed for the incomplete straightening of the fibre once passed through the hook
85 inflection point.

86 In addition to these analytical and semi-analytical solutions, empirical and numerical models
87 were developed. For example, Laranjeira et al. (2010a, b) used pull-out test results to identify
88 the generic shape of a single fibre load-slip response and provided rules for the translation and
89 superposition of this general shape to allow for variations in fibre inclination and the presence
90 of hooks. Zhan and Meschke (2014) improved the approach of Laranjeira et al. (2010a, b) by
91 developing a mechanical model for the hook contribution. The forces and moments in the
92 hooked end were calculated for a number of key states as the slip of the free end increases. This
93 was achieved by considering force equilibrium as well as the shear, moment and axial
94 capacities of the fibre. An additional frictional force is also considered for the incompletely
95 straightened section of fibre. This model also considers the detailed geometry of the bends of
96 the fibre.

97 Considering numerical models, Zhang et al. (2016) developed a model for inclined fibres using
98 cohesive elements with a mixed mode fracture criterion to represent the bond-slip behaviour at
99 the interface. A generic constitutive model for the interfacial bond-shear stress relationship was

proposed considering the effect of internal physical and chemical cohesion, fibre surface-roughness and concrete spalling at the loading end.

Based on the above review, it is identified that there is a need for the development of an analytical predictive model that can accommodate the transfer of interfacial bond stresses throughout the entire pull-out process, thereby avoiding the need for a smoothing polynomial. Further, it is advantageous to consider the behaviour of the hook directly as a function of fibre geometry and material properties to avoid the need for empirical calibration testing for each new fibre type.

To address this need, a partial-interaction based analytical model developed by Sturm et al. (2019) for simulating interface of an externally bonded plate with mechanical anchors is adapted in this paper for modelling the pull-out behaviour of a single fibre with and without hooks. The concept proposed by Sturm et al. (2019) is ideal for modification and application to the fibre pull-out problem because: (i) it explicitly considers the combined action of bond stress along the interface and the discrete change in force from the mechanical anchors throughout the entire loading scenario; and (ii) the matrix formulation can be applied to accommodate any number of discrete forces arising from mechanical anchorages without any need for defining new load cases. While deemed to be ideal for application, Sturm et al. (2019)'s required modification as follows:

(1) The bi-linear bond-slip relationship (linear ascending for elastic response and linear descending for de-bonding) needs to be replaced with a tri-linear bond-slip relationship to accommodate the contribution of friction (linear ascending, linear descending, and a constant friction).

(2) The dowel action mechanism used to simulate mechanical anchors in plates does not apply for embedded fibres and needs to be replaced with a plastic hinge model to facilitate bending of the fibre near a hook.

Mechanics for pull-out behaviour of fibres utilising partial interaction mechanisms

Fig. 1(a) shows a typical single straight fibre pull-out test scenario in which the fibre is subjected to a pull-out force P_{f1} while the concrete specimen is supported at the loaded end. The load-slip (P_f -Δ) relationship of the fibre can be quantified using the same governing partial-interaction (PI) mechanics that have been applied to predict interfacial bond-slip models in reinforced concrete, steel concrete composites and retrofitted structures (Strum and Visintin 2019, Turkmen et al. 2020).

Fig. 1(b) shows the variation of interface bond shear stress τ along the bonded length, where P_f can be expressed as the integral of the bond stress τ over the bonded area (bonded length multiplied by perimeter of the fibre). Fig. 1(c) shows the distribution of interface shear slip δ (local slip) that can be used to evaluate bond stress using bond stress-slip (τ-δ) relationship as shown in Fig. 1(d), which is a fundamental material property unique to a given combination of concrete and fibre type and must be quantified experimentally, by a single fibre pull-out tests.

To quantify the distributions of shear stress and slip in Fig. 1(b) and Fig. 1(c), the specimen (fibre and concrete as in Fig. 1(a)) is discretised into infinitesimal elements of length dx along the embedded length L as show in Fig. 1(e). The analysis is undertaken iteratively, and to initiate the process, the value of the load P_f required to cause a specified value of Δ is first assumed; in Fig 1(e) this force is defined as P_{f1}, located on the upper side of element 1. Based on the equilibrium of the whole specimen, the load acting on concrete at the upper side of the first element P_{c1} is also equal to P_{f1}.

With a specified value of slip the upper side of the first element $\delta_{(1)}=\Delta$, the bond stress $\tau_{(1)}$ can be determined using the τ-δ relationship as given in Fig. 1(d). Integration of $\tau_{(1)}$over the bonded area (assuming it to be uniform over the infinitesimal element length dx), the bond force transferred from the fibre to the concrete over the first element B_1 is $\tau_{(1)}L_p dx$, where L_p is the bonded perimeter of the fibre.

Applying force equilibrium over the element, the force at the bottom surface of the fibre P_{f2} in Fig. 1(e) is $P_{f2}=P_{f1} - B_1$ and the corresponding force on concrete is $P_{c2} = P_{c1} + B_1$. These forces (P_{f2} and P_{c2}) are also taken to act on the upper side of the next (second) element in Fig. 1(e), which will be required for subsequent calculations.

The axial strain of the first element fibre (ε_{f1}) and concrete (ε_{c1}) are taken to arise from the average force in the fibre and concrete over the element length i.e., $(P_{f1}+P_{f2})/2E_fA_f$ and $(P_{c1}+P_{c2})/2E_cA_c$ and the difference in strain between the fibre and the surrounding concrete is the rate of change in local slip along x. That is, the slip strain is defined as $(d\delta/dx)_1 = \varepsilon_{f1} - \varepsilon_{c1}$ for the first element. Integration of slip strain over the element length dx gives the change in slip that occurs over the element length $\Delta\delta_1 = (\varepsilon_{f1} - \varepsilon_{c1})\, dx$, which can be subtracted from the slip at the top side of the element to give the slip at its bottom ($\delta_{(2)} = \delta_{(1)} - \Delta\delta_1$). This slip is also taken to the slip at the top side of the next element i.e. element 2.

The above process is applied to the subsequent elements, starting from the loaded end to quantify the local fields of stress, strain and slip along the fibre length for a specified global slip Δ and assumed fibre pull-out load P_f. The above process is again repeated by varying the fibre force P_f for an imposed slip Δ until the boundary conditions are satisfied. The boundary condition may be zero slip and zero slip strain within any point within the fibre length or zero slip strain at the end of fibre depending on if a point of full-interaction (zero slip) occurs along

the fibre length, or if it is slipping along the full fibre length. The computational implementation of the above process is shown in the form of a flow chart in Fig. 2.

Modelling for the contribution of hook

Now let us consider the additional contribution to the P_f/Δ behaviour provided by a hook, where for the purpose of this explanation the hook is taken to comprise of two bends as shown in Fig. 3(a). Although only a double bend hook is considered here, the same approach can be extended and applied to any number of hooks along the fibre length.

As the fibre is pulled, bond stresses develop along the fibre length in the same way as that of a straight fibre, but additional forces are developed at the location of bends as shown in Fig. 3(b) and (c). These forces include:

(1) Those generated at the bends arising from the change in fibre orientation. These forces are comprised of a force N acting normal to the inclined segment of the fibre and a tangential frictional force μN, where μ is the frictional coefficient.

(2) The bending associated with straightening of the fibre, as it is pulled through the apex of a bend necessitates formation of a plastic hinge at the location of bend. The force generated at the location of the plastic hinge is taken as F_{PH} in Fig. 3.

Change in axial force of the fibre at the bends

Let us now consider the change in axial force that occur at the location of a bend. For the purpose of the derivation, any parameter immediately before or after a bend is indicated by negative and positive superscripts respectively (l_1^- and l_1^+). Horizontal and vertical force equilibrium are applied to quantify the relationship between the axial force in the fibre at the two sides of the first bend ($F_f(l_1^-)$ and $F_f(l_1^+)$) in terms of F_{PH}, μ, and θ as follows.

$$0 = -N_1 \cos(\theta) + [F_{\mathrm{f}}(l_1^+) - \mu N_1 - F_{\mathrm{PH}}] \sin(\theta) \quad (1)$$

$$0 = F_{\mathrm{f}}(l_1^-) - N_1 \sin(\theta) - [F_{\mathrm{f}}(l_1^+) - \mu N_1 - F_{\mathrm{PH}}] \cos(\theta) \quad (2)$$

Eq. (1) can be rearranged to give the normal force N_1 in terms of the remaining parameters

$$N_1 = \frac{[F_{\mathrm{f}}(l_1^+) - F_{\mathrm{PH}}] \sin(\theta)}{\cos(\theta) + \mu \sin(\theta)} \quad (3)$$

and substitution of Eq. (3) into Eq. (2) gives the relationship between $F_{\mathrm{f}}(l_1^+)$ and $F_{\mathrm{f}}(l_1^-)$

$$F_{\mathrm{f}}(l_1^+) = F_{\mathrm{f}}(l_1^-)[\cos(\theta) + \mu \sin(\theta)] + F_{\mathrm{PH}} \quad (4)$$

Similarly, applying horizontal and vertical force equilibrium at the second bend

$$-F_{\mathrm{f}}(l_2^-) \sin(\theta) + N_2 \cos(\theta) - \mu N_2 \sin(\theta) = 0 \quad (5)$$

$$F_{\mathrm{f}}(l_2^-) \cos(\theta) + N_2 \sin(\theta) + \mu N_2 \cos(\theta) - [F_{\mathrm{f}}(l_2^+) - F_{\mathrm{PH}}] = 0 \quad (6)$$

Eq. (5) can then be rearranged to give normal force N_2

$$N_2 = \frac{F_{\mathrm{f}}(l_2^-) \sin(\theta)}{\cos(\theta) - \mu \sin(\theta)} \quad (7)$$

and substituting Eq. (7) into Eq. (6) the relationship between $F_{\mathrm{f}}(l_2^+)$ and $F_{\mathrm{f}}(l_2^-)$ is

$$F_{\mathrm{f}}(l_2^+) = \frac{F_{\mathrm{f}}(l_2^-)}{\cos(\theta) - \mu \sin(\theta)} + F_{\mathrm{PH}} \quad (8)$$

Hence Eqs. (4) and (8) give the step change in the force of the fibre at the location of two bends in terms of F_{PH}, μ, and θ.

Force due to formation of plastic hinge (F_{PH})

206 Based on the concept of Alwan et al. (1999), the additional force in the fibre at a bend due to
207 the formation of plastic hinge required to straighten the fibre as it is pulled through the the bend
208 is

209 $$F_{\mathrm{PH}} = \frac{M_{\mathrm{PH}}}{d_{\mathrm{f}} \cos\theta} \tag{9}$$

210 In which M_{PH} is the moment to produce the plastic hinge, which is assumed to form over a
211 length equal to the fibre diameter (d_{f}), and θ is the rotation of the plastic hinge, which is equal
212 to the bend angle (Fig. 4).

213 For the purpose of the following derivation it is assumed that the fibre has a circular cross-
214 section, but the generic approach can be applied to any shape fibre. The cross-section of the
215 fibre is taken to be in an elastoplastic state (Fig. 4(b)) such that the moment M_{PH} can be related
216 to the curvature χ in Fig. 4(c), and further to the hinge rotation (θ) in Fig. 4(a) using the hinge
217 length (d_{f})

218 $$\chi = \frac{\theta}{d_{\mathrm{f}}} \tag{10}$$

219 Considering the strain profile in Fig. 4(c), at a point along the fibre depth the strain is $\varepsilon_{\mathrm{f}} = \chi y$
220 where y is the distance of the point from neutral axis (N.A.). If there is no yielding of the section
221 the stress profile remains linear as in Fig. 4(d) and the moment can be determined using linear
222 elastic theory

223 $$M = E_{\mathrm{f}} I_{\mathrm{f}} \chi = E_{\mathrm{f}} \left(\frac{\pi}{64} d_{\mathrm{f}}^4\right) \chi \tag{11}$$

224 In which E_{f} is the elastic modulus of the fibre, and I_{f} is the second moment of area of the fibre
225 section.

Eq. (11) is applicable until the outer layer of the fibre yields at a strain ε_y, corresponding to a moment M_y. Based on standard sectional analysis, at the initiation of yield the curvature χ_y and corresponding moment are:

$$\chi_y = 2\frac{\varepsilon_y}{d_f} \tag{12}$$

$$M_y = f_y \frac{\pi}{32} d_f^3 \tag{13}$$

Any further increases in curvature beyond χ_y cause the depth of the yielding section to propagate towards the centre of the fibre. Assuming the steel fibre be elastic-perfectly-plastic, the stress profile has a shape as shown in Fig. 4(e) and can be described by

$$\sigma = \begin{cases} f_y; |y| > y_1 \\ E_f \chi y; \ |y| < y_1 \end{cases} \tag{14}$$

Where f_y is the yield stress, and y_1 is the extent of elastic region measured from the neutral axis and is given by

$$y_1 = \frac{\varepsilon_y}{\chi} = \frac{\chi_y}{\chi}\frac{d_f}{2} \tag{15}$$

Eq. (14) can be used to determine the post yielding moment M_{PH} by integrating the elemental moment produced by the distribution stress (Fig. 4(e)) over the cross-section about the neutral axis to give

$$M_{PH} = \int \sigma y \, dA = E_f \chi \int_{A_e} y^2 \, dA + f_y \int_{A_p} y \, dA \tag{16}$$

where A_e is the area of elastic region of the cross-section, and A_p is the area of plastic region.

For the circular geometry of the fibre (Fig. 4(b)), Eq. (16) can be rewritten as

244 $$M_{\mathrm{PH}} = 4E_{\mathrm{f}}\chi \int_0^{y_1} y^2 \sqrt{\left(\frac{d_{\mathrm{f}}}{2}\right)^2 - y^2}\, dy + 4f_y \int_{y1}^{d_{\mathrm{f}}/2} y \sqrt{\left(\frac{d_{\mathrm{f}}}{2}\right)^2 - y^2}\, dy \quad (17)$$

245 Which upon integration gives:

246 $$M_{\mathrm{PH}} = E_f \chi \frac{d_{\mathrm{f}}^4}{32}\left\{\arcsin\frac{\chi_y}{\chi} - \frac{\chi_y}{\chi}\left[1 - \left(\frac{\chi_y}{\chi}\right)^2\right]^{\frac{3}{2}} + \left(\frac{\chi_y}{\chi}\right)^3 \sqrt{1 - \left(\frac{\chi_y}{\chi}\right)^2}\right\} + f_y \frac{d_{\mathrm{f}}^3}{6}\left[1 - \left(\frac{\chi_y}{\chi}\right)^2\right]^{\frac{3}{2}}$$

247 (18)

248 Using Eqs. (13) and (18), the variation of $M_{\mathrm{PH}}/M_{\mathrm{y}}$ with χ/χ_{y} for a specific fibre is shown in Fig.
249 5. Having now derived the plastic hinge moment in Eq. (18), the additional force in the fibre at
250 the apex of the hook due to the plastic hinge formation F_{PH} is given by substituting Eq. (18)
251 into Eq. (9).

252 A limitation of the plastic hinge approach is that the force F_{PH} is applied as a step change rather
253 than gradually increasing as a given portion of the fibre pulls through the apex of the bend. The
254 result of this approximation is that a step change in fibre force occurs at the global $P_{\mathrm{f}} - \Delta$ level.
255 These step changes are not observed experimentally and so Alwan et al. (1999) suggest fitting
256 a smoothing polynomial to the $P_{\mathrm{f}} - \Delta$ curve. An alternative approach is applied here, in which
257 the force F_{PH} is expressed in terms of slip δ according to Eq. (19a), (19b), (19c).

258 $$F_{\mathrm{PH}} = \begin{cases} \dfrac{\delta}{\left(\frac{d_{\mathrm{f}}}{2}\right)} \dfrac{M_{\mathrm{PH}}}{d_{\mathrm{f}}\cos(\theta)} & if\ \delta < \dfrac{d_{\mathrm{f}}}{2} \quad (19a) \\ \dfrac{l_{\mathrm{m}} - \delta_0}{2d_{\mathrm{f}}} \dfrac{M_{\mathrm{PH}}}{d_{\mathrm{f}}\cos(\theta)} & if\ \delta_0 > l_{\mathrm{m}} - 2d_{\mathrm{f}} \quad (19b) \\ \dfrac{M_{\mathrm{PH}}}{d_{\mathrm{f}}\cos\theta} & if\ \delta > \dfrac{d_{\mathrm{f}}}{2}\ and\ \delta_0 < l_{\mathrm{m}} - 2d_{\mathrm{f}} \quad (19c) \end{cases}$$

259 where l_{m} is the distance along the fibre from the free end (m = 1 for the Bend 1 and m = 2 for
260 the Bend 2).

The relationship between the slip of the fibre and F_{PH} in Eq. 19 is suggested as it allows the force to be zero when the slip is zero and then to increase gradually until the maximum plastic hinge force is reached. It further allows the force to reduce gradually as the end of the fibre moves past the bend of the fibre. This simple linear approximation is it captures the gradual increase and decrease in F_{PH} that should occur as the plastic hinge which has a defined length moves through the apex of the bend, which is taken to have an infinitesimal length.

The flow chart in Fig. 2 also shows the computational implementation of the above process applicable for hooked fibres.

Analytical solution of the pull-out response

Above sections provided a generic numerical solution technique to obtain the load-slip behaviour of a single straight and hooked fibre. The numerical scheme presented is generic in that it can accommodate any shape bond slip relationship (Fig. 1(d)) but is limited in that it requires an iterative solution technique, which may complicate implementation. Hence in this section an analytical solution is derived based on the application of a simplified (idealised) tri-linear bond slip relationship (Fig. 6(a)).

As described in the numerical modelling, the slip strain at any point can be written as the difference between the fibre and concrete strains at that point:

$$\frac{d\delta}{dx} = \frac{F_f}{E_f A_f} - \frac{F_c}{E_c A_c} \tag{20}$$

where A_f and A_c are the cross-sectional area of the fibre and concrete, E_f and E_c are elastic modulus of the fibre and concrete. It should be noted that to simplify the mathematical derivation x is measured from the free-embedded end of the fibre (Fig. 6(b), (c)) rather than from the loaded end as in the numerical model.

The differentiation of Eq. (20) with respect to *x* gives

$$\frac{d^2\delta}{dx^2} = \frac{1}{E_\mathrm{f}A_\mathrm{f}}\frac{dF_\mathrm{f}}{dx} - \frac{1}{E_\mathrm{c}A_\mathrm{c}}\frac{dF_\mathrm{c}}{dx} \tag{21}$$

where the rate of change in the axial force of fibre and concrete can be obtained from the force equilibrium of an element (Fig. 1(e)) as follows.

$$\frac{dF_\mathrm{f}}{dx} = \tau L_\mathrm{p} \tag{22}$$

$$\frac{dF_\mathrm{c}}{dx} = -\tau L_\mathrm{p} \tag{23}$$

Substituting Eqs. (22) and (23) into Eq. (21), it gives the classical governing equation for partial interaction mechanism (Volkersen, 1938) as

$$\frac{d^2\delta}{dx^2} = \tau\,\beta \tag{24}$$

where,

$$\beta = \frac{L_\mathrm{p}}{EA_\mathrm{eff}} \tag{25}$$

and

$$EA_\mathrm{eff} = \frac{1}{\left(\frac{1}{E_\mathrm{f}A_\mathrm{f}} + \frac{1}{E_\mathrm{c}A_\mathrm{c}}\right)}. \tag{26}$$

Eq. (24) was used and solved for various problems such as bond slip response of straight internal reinforcing bars within concrete, rock bolts, and external plates and sheets for retrofitting existing members using a range of approximations for the local bond stress slip relationship, but the solution of this equation for modelling a fibre with a hook is yet to be established.

To develop a specific solution to Eq. (24), it requires the variation of local bond shear stress (τ) in terms of shear slip (δ). For the development of closed-form analytical solutions the nonlinear stress-slip relationship in Fig. 6(a) is idealised as a tri-linear relationship with three zones

$$\tau(\delta) = \begin{cases} k\,\delta & \text{Zone I, i. e. } \delta \le \delta_1 \quad (27a) \\ \tau_{\mathrm{f}} - k_{\mathrm{d}}(\delta - \delta_1) & \text{Zone II, i. e. } \delta_1 < \delta \le \delta_2 \quad (27b) \\ \tau_{\mathrm{r}} & \text{Zone III, i. e. } \delta > \delta_2 \quad (27c) \end{cases}$$

In which,

$$k = \frac{\tau_{\mathrm{f}}}{\delta_1} \tag{28}$$

and

$$k_{\mathrm{d}} = \frac{\tau_{\mathrm{f}} - \tau_{\mathrm{r}}}{\delta_2 - \delta_1} \tag{29}$$

Having defined a τ-δ relationship Eq. (24) can be solved by applying appropriate boundary conditions as following Eqs. (30) and (33).

Rearranging Eq. (20), at the loaded end the slip strain can be defined as a proportion of the fibre force

$$\left.\frac{d\delta}{dx}\right|_{\mathrm{x=L}} = P_{\mathrm{f}}\left(\frac{1}{E_{\mathrm{f}}A_{\mathrm{f}}} + \frac{1}{E_{\mathrm{c}}A_{\mathrm{c}}}\right) = \frac{P_{\mathrm{f}}}{EA_{\mathrm{eff}}} \tag{30}$$

where,

$$P_{\mathrm{f}} = F_{\mathrm{f}} = F_{\mathrm{c}} \tag{31}$$

and

$$EA_{\mathrm{eff}} = \frac{1}{\frac{1}{E_{\mathrm{f}}A_{\mathrm{f}}} + \frac{1}{E_{\mathrm{c}}A_{\mathrm{c}}}} \tag{32}$$

Assuming that the fibre will slip along the entire length, at the free end

$$\left.\frac{d\delta}{dx}\right|_{x=0} = 0 \tag{33}$$

Derivations for straight fibre pull-out

Having established the governing equations describing the fields of slip and slip strain, it is now a matter of applying the boundary conditions to derive a specific solution. Since the τ-δ relationship has three linear portions a specific solution needs to be obtained for each zone in Fig. 6(a).

In a recent study by Sturm et al. (2019), the governing equation with identical boundary conditions has been solved to quantify the load-slip behaviour of FRP plates adhesively bonded and mechanically anchored to reinforced concrete. The specific solution presented by Sturm et al. (2019) is useful in the present investigation as it can be utilised and extended to solve the present problem. The first step in this extension is to allow for post debonding friction (zone III) which was absent in the original solution by Sturm et al. (2019). Hence the primary focus of this section is to incorporate the contributions of zone III for a straight fibre before incorporating the influence of hooks in the following section. Though analytical solutions, considering the three zones, have been derived e.g. by Vaculik et al. (2018), the matrix formulation of Sturm et al. (2019) is preferred in deriving the present model as it allows for a more convenient incorporation of multiple hooks. That is, the general matrix form can be easily expanded rather than needing to derive specific solutions for each individual combination of load cases and number of hooks.

In the remainder of the derivation, solutions for slip and slip strain are presented for each zone in a matrix form which consists of solution matrix, position vector and unknown coefficient vector. The free end boundary conditions are first used to get the coefficient vector for the three

zones when the bond stress over the entire fibre length will be governed by a single zone. In a more complex scenario, where different zones (linear elastic, softening and residual friction) will govern the different parts of the fibre length, the location of the transition points between two zones are determined, which enables the establishment of the coefficient vector. It is then shown how the equations can be applied to quantify the load slip behaviour of the fibre at the loaded end by imposing a slip at the free end.

Solution for Zone I ($\delta \leq \delta_1$)

The solution for Zone I can be derived by substituting Eq. (27a) into Eq. (24), which gives the linear ordinary differential equation

$$\frac{d^2\delta}{dx^2} = k\beta\delta \tag{34}$$

The above equation will have homogeneous solution

$$\delta = c_1\, sinh(\lambda_1 x) + c_2\, cosh(\lambda_1 x) \tag{35}$$

In which

$$\lambda_1 = \sqrt{k\beta} \tag{36}$$

Differentiating the equation for local slip (Eq. (35)), the slip-strain can be expressed as

$$\frac{d\delta}{dx} = \lambda_1[c_1\, cosh(\lambda_1 x) + c_2\, sinh(\lambda_1 x)] \tag{37}$$

Eqs. (35) and (37) can be written in matrix form as

$$\begin{bmatrix} \delta \\ \frac{d\delta}{dx} \end{bmatrix} = \begin{bmatrix} sinh(\lambda_1 x) & cosh(\lambda_1 x) \\ \lambda_1 cosh(\lambda_1 x) & \lambda_1 sinh\,(\lambda_1 x) \end{bmatrix} \begin{bmatrix} c_1 \\ c_2 \end{bmatrix} = \boldsymbol{S_1\, c_1} \tag{38}$$

where $\boldsymbol{S_1}$ and $\boldsymbol{c_1}$ (boldface indicates matrix and vector quantities) are defined as solution matrix and coefficient vector, respectively for Zone I.

The coefficient vector $\boldsymbol{c}$ can be quantified by applying the free end ($x = 0$) boundary conditions ($\delta|_{x=0} = \delta_0$ and $(d\delta/dx)|_{x=0} = 0$) in Eq. (38).

$$\begin{bmatrix} \delta_0 \\ 0 \end{bmatrix} = \begin{bmatrix} 0 & 1 \\ \lambda_1 & 0 \end{bmatrix} \begin{bmatrix} c_1 \\ c_2 \end{bmatrix} \tag{39}$$

Therefore, the coefficient vector for Zone I $\delta_0 < \delta_1$ is

$$\boldsymbol{c_1} = \begin{bmatrix} 0 \\ \delta_0 \end{bmatrix} = \delta_0 \begin{bmatrix} 0 \\ 1 \end{bmatrix} = \delta_0 \, \boldsymbol{e_1} \tag{40}$$

where $\boldsymbol{e_1} = [0 \quad 1]^{\mathrm{T}}$

Solution for Zone II ($\boldsymbol{\delta_1 < \delta \leq \delta_2}$)

The solution for Zone II can be derived by substituting Eq. (27b) into Eq. (24) which gives the linear second order ordinary differential equation as

$$\frac{d^2\delta}{dx^2} = (\tau_{\mathrm{f}} + k_{\mathrm{d}}\delta_1)\beta - k_{\mathrm{d}}\beta\delta \tag{41}$$

The Eq. (41) has a homogeneous solution and a particular integral as follows

$$\delta = c_1 \sin(\lambda_2 x) + c_2 \cos(\lambda_2 x) + \delta_{\mathrm{p}} \tag{42}$$

where

$$\lambda_2 = \sqrt{k_{\mathrm{d}}\beta} \tag{43}$$

and

$$\delta_{\mathrm{p}} = \delta_1 + \tau_{\mathrm{f}}/k_{\mathrm{d}}. \tag{44}$$

Differentiation of Eq. (42) gives the slip strain

$$\frac{d\delta}{dx} = \lambda_2 c_1 \cos(\lambda_2 x) - \lambda_2 c_2 \sin(\lambda_2 x) \tag{45}$$

Now rewriting Eqs. (42) and (30) in matrix form yields

$$\begin{bmatrix} \delta \\ \frac{d\delta}{dx} \end{bmatrix} = \begin{bmatrix} \sin(\lambda_2 x) & \cos(\lambda_2 x) \\ \lambda_2 \cos(\lambda_2 x) & -\lambda_2 \sin(\lambda_2 x) \end{bmatrix} \begin{bmatrix} c_1 \\ c_2 \end{bmatrix} + \delta_{\mathrm{p}} \begin{bmatrix} 1 \\ 0 \end{bmatrix} = \boldsymbol{S_2}\, \boldsymbol{c_2} + \delta_p\, \boldsymbol{e_2} \tag{46}$$

where $\boldsymbol{e_2} = [1 \quad 0]^T$, $\boldsymbol{S_2}$, and $\boldsymbol{c_2}$ are the solution matrix and coefficient vector, respectively for Zone II.

The coefficient vector $\boldsymbol{c_2}$ (Eq. (46)) for this zone can be determined with the same boundary conditions as used in Zone I. Thus, substituting slip and slip-strain at $x = 0$ into Eq. (46), it gives

$$\begin{bmatrix} \delta_0 \\ 0 \end{bmatrix} = \begin{bmatrix} 0 & 1 \\ \lambda_2 & 0 \end{bmatrix} \begin{bmatrix} c_1 \\ c_2 \end{bmatrix} + \delta_p \begin{bmatrix} 1 \\ 0 \end{bmatrix} \tag{47}$$

where c_1 and c_2 can be derived from Eq. (47) as $c_1 = 0$ and $c_2 = \delta_0 - \delta_p$.

Thus, the coefficient vector for Zone II ($\delta_1 < \delta \leq \delta_2$) can be written as

$$\boldsymbol{c_2} = \begin{bmatrix} c_1 \\ c_2 \end{bmatrix} = \begin{bmatrix} 0 \\ \delta_0 - \delta_p \end{bmatrix} = (\delta_0 - \delta_p) \begin{bmatrix} 0 \\ 1 \end{bmatrix} = (\delta_0 - \delta_p)\, \boldsymbol{e_1} \tag{48}$$

Solution for Zone III ($\boldsymbol{\delta > \delta_2}$)

Zone III consists only of a constant frictional branch ($\tau = \tau_{\mathrm{r}}$ in Fig. 6(a)), hence substitution of $\tau = \tau_{\mathrm{r}}$ in Eq. (24) gives

$$\frac{d^2\delta}{dx^2} = \tau_r \beta \tag{49}$$

The slip strain and slip can be obtained by integrating Eq. (49) to give

$$\frac{d\delta}{dx} = \tau_r \beta x + c_1 \tag{50}$$

and further integrating Eq. (50) gives the distribution of slip

$$\delta = \tau_r \beta \frac{x^2}{2} + c_1 x + c_2 \tag{51}$$

Both of which can again be expressed in matric form as

$$\begin{bmatrix} \delta \\ \frac{d\delta}{dx} \end{bmatrix} = \begin{bmatrix} x^2/2 \\ x \end{bmatrix} \tau_r \beta + \begin{bmatrix} x & 1 \\ 1 & 0 \end{bmatrix} \begin{bmatrix} c_1 \\ c_2 \end{bmatrix} = \boldsymbol{r}\, \tau_r \beta + \boldsymbol{S_3}\, \boldsymbol{c_3} \tag{52}$$

where $\boldsymbol{r}$ is defined as the position vector, and $\boldsymbol{S_3}$ and $\boldsymbol{c_3}$ are solution matrix and coefficient vector, respectively for Zone III.

The coefficient vector $\boldsymbol{c_3}$ (Eq. (52)) can be obtained by imposing the same boundary condition at the free end as used for the solution for Zone I, to give

$$\begin{bmatrix} \delta_0 \\ 0 \end{bmatrix} = \begin{bmatrix} 0 & 1 \\ 1 & 0 \end{bmatrix} \begin{bmatrix} c_1 \\ c_2 \end{bmatrix} \tag{53}$$

Solution of Eq. 53 gives $c_1 = 0$, and $c_2 = \delta_0$, which can be expressed in matrix form as

$$\boldsymbol{c_3} = \begin{bmatrix} 0 \\ \delta_0 \end{bmatrix} = \delta_0 \begin{bmatrix} 0 \\ 1 \end{bmatrix} = \delta_0\, \boldsymbol{e_1} \tag{54}$$

The solutions for Zone I, Zone II and Zone III provided by Eqs. (40), (48) and (54) respectively are only applicable when the distribution of bond stress along the entire fibre length is restricted

to that of a single zone. If the slip at the loaded end is less than δ_1, the bond stress provided by Zone I will be applicable for the entire fibre length. When this slip is greater than δ_1, the distribution of bond stress along the fibre length will be provided by the different zones. To develop a generic solution, it is therefore necessary to identify the locations of the transition of these zones along the fibre length.

Solution for Zone I-II transition ($x = x_1$)

The distance of the first transition (between zone I and zone II) from the free end x_1 occurs when the slip is equal to δ_1. Substituting $x = x_1$ and $\delta = \delta_1$ into Eq. (35), it gives

$$\delta_1 = c_1 \sinh(\lambda_1 x_1) + c_2 \cosh(\lambda_1 x_1) \tag{55}$$

For the convenience of solution, the hyperbolic trigonometric functions in Eq. (55) are expressed in their exponential forms (Olver et al., 2020) to give

$$\delta_1 = e^{\lambda_1 x_1}\left(\frac{c_1+c_2}{2}\right) + e^{-\lambda_1 x_1}\left(\frac{c_2-c_1}{2}\right) \tag{56}$$

The above equation can be rearranged to express as a quadratic equation in terms of $e^{\lambda_1 x_1}$

$$\left(\frac{c_1+c_2}{2}\right)\left(e^{\lambda_1 x_1}\right)^2 - \delta_1\left(e^{\lambda_1 x_1}\right) + \left(\frac{c_2-c_1}{2}\right) = 0 \tag{57}$$

The standard solution of the quadratic equation (Eq. (57)) considering the positive part of the discriminant is

$$e^{\lambda_1 x_1} = \frac{\delta_1 + \sqrt{\delta_1^2 + c_1^2 - c_2^2}}{c_1 + c_2} \tag{58}$$

Eq. (58) can then be solved to describe the distance of transition point from the free end x_1 as

$$x_1 = \frac{1}{\lambda_1}\ln\left(\frac{\delta_0 + \sqrt{\delta_0^2 + c_1^2 - c_2^2}}{c_1 + c_2}\right) \tag{59}$$

At the transition between Zone I and Zone II, the slip and slip-strain are continuous, hence equating Eqs. (38) and (46) gives

$$\boldsymbol{S_1}|_{x=x_1}\,\boldsymbol{c_1} = \boldsymbol{S_2}|_{x=x_1}\,\boldsymbol{c_2} + \delta_p\,\boldsymbol{e_2} \tag{60}$$

and the coefficient vector for Zone II is

$$\boldsymbol{c_2} = (\boldsymbol{S_2})^{-1}|_{x=x_1}\,\boldsymbol{S_1}|_{x=x_1}\boldsymbol{c_1} - \delta_p(\boldsymbol{S_2})^{-1}|_{x=x_1}\boldsymbol{e_2} \tag{61}$$

Solution for Zone II-III transition ($x = x_2$)

The distance of the second transition (between Zone II and Zone III) from the free end is defined as x_2 where the slip is δ_2. Substituting $x = x_2$ and $\delta = \delta_2$ in Eq. (42), it gives

$$\delta_2 = c_1\sin(\lambda_2 x_2) + c_2\cos(\lambda_2 x_2) + \delta_\mathrm{p} \tag{62}$$

Eq. (62) can be rewritten by replacing the sine and cosine terms with equivalent tangent terms to obtain the quadratic equation in terms of $\tan\left(\frac{\lambda_2 x_2}{2}\right)$

$$\left(c_2 - \delta_p + \delta_2\right)\tan^2\left(\frac{\lambda_2 x_2}{2}\right) - 2c_1\tan\left(\frac{\lambda_2 x_2}{2}\right) - \left(c_2 + \delta_p - \delta_2\right) = 0 \tag{63}$$

Solving Eq. (63) for the transition point x_2 gives

$$x_2 = \frac{2}{\lambda_2}\left\{\arctan\left[\frac{c_1 - \sqrt{c_1^2 + c_2^2 - (\delta_2 - \delta_p)^2}}{c_2 + \delta_2 - \delta_\mathrm{p}}\right]\right\} \tag{64}$$

At the Zone II-III transition, slip and slip-strain are again continuous, such that equating Eqs. (46) and (52) gives

$$\boldsymbol{S_2}|_{x=x_2}\,\boldsymbol{c_2} + \delta_p\,\boldsymbol{e_2} = \boldsymbol{r}|_{x=x_2}\,\tau_r\,\beta + \boldsymbol{S_3}|_{x=x_2}\,\boldsymbol{c_3} \quad (65)$$

So the coefficient vector for Zone III can be obtained from that of Zone II by rewriting the Eq. (65) as

$$\boldsymbol{c_3} = (\boldsymbol{S_3})^{-1}|_{x=x_2}\,\boldsymbol{S_2}|_{x=x_2}\,\boldsymbol{c_2} + \delta_p\,(\boldsymbol{S_3})^{-1}|_{x=x_2}\,\boldsymbol{e_2} - (\boldsymbol{S_3})^{-1}|_{x=x_2}\,\boldsymbol{r}|_{x=x_2}\,\tau_r\,\beta \quad (66)$$

Application of the above components for final solution of global load-slip (P_f-Δ)

The expressions derived in the previous sections can be used parametrically to determine the global load-slip (P_f-Δ) relationship from the imposed free end slip δ_0, which is increased incrementally to provide the full range P_f-Δ relationship. The overall procedure for doing so is summarised in Fig. 7 as follows:

1) A free end slip δ_{0i} is imposed on the fibre.

2) The fibre embedment length L is reduced by the free end slip δ_{0i}.

3) The initial values of the coefficient vectors are defined using δ_{0i} and the boundary condition $\frac{d\delta}{dx} = 0$ at the free end.

4) A check is made to identify if a transition point between zones occurs before reaching the end of the fibre.

5) If a transition point is reached before the end of the fibre, the coefficient vectors in step 3 are updated to allow for the presence of multiple zones.

6) Once the coefficient vector is known, at the loaded end, Δ and $\frac{d\delta}{dx}$ can be determined and from $\frac{d\delta}{dx}$ the force in fibre P_{f_i} is also known.

Derivations for hooked fibre pull-out

The change of fibre force that occurs at the bends is given by Eqs. (4) and (8), and this step change results in a change in slip strain across the bend equal to

$$\left.\frac{d\delta}{dx}\right|^{+} - \left.\frac{d\delta}{dx}\right|^{-} = \frac{F_{\mathrm{f}}(l^{+}) - F_{\mathrm{f}}(l^{-})}{EA_{\mathrm{eff}}} \tag{67}$$

Substituting Eq. (4) for $F_{\mathrm{f}}(l^{+})$ in Eq. (67) gives the slip strain at the first bend as

$$\left.\frac{d\delta}{dx}\right|_{l_1}^{+} - \left.\frac{d\delta}{dx}\right|_{l_1}^{-} = \frac{F_{\mathrm{f}}(l_1^{-})[\cos(\theta) + \mu\sin(\theta) - 1] + F_{\mathrm{PH}}}{EA_{\mathrm{eff}}} \tag{68}$$

Similarly substituting in Eq. (8) for $F_{\mathrm{f}}(l^{+})$ gives the change in the slip strain at second bend as

$$\left.\frac{d\delta}{dx}\right|_{l_2}^{+} - \left.\frac{d\delta}{dx}\right|_{l_2}^{-} = \frac{F_{\mathrm{f}}(l_2^{-})\left[\frac{1}{\cos(\theta) - \mu\sin(\theta)} - 1\right] + F_{\mathrm{PH}}}{EA_{\mathrm{eff}}} \tag{69}$$

The change of coefficient vectors at the bends are now required to redefine for the three zones.

Change of coefficient vectors at bends for Zone I, II, and III

The change of coefficient vectors at a bend can be calculated using Eqs (38), (46), and (52).

The slip and slip-strain immediately before and after a bend for Zone I, can be written in matrix form as

$$\begin{bmatrix} \delta^{-} \\ \left.\frac{d\delta}{dx}\right|^{-} \end{bmatrix} = \boldsymbol{S_1 c_1^{-}} \tag{70}$$

and

$$\begin{bmatrix} \delta^{+} \\ \left.\frac{d\delta}{dx}\right|^{+} \end{bmatrix} = \boldsymbol{S_1 c_1^{+}} \tag{71}$$

The change of coefficient vector is therefore

$$\boldsymbol{c_1^+} - \boldsymbol{c_1^-} = \left(\boldsymbol{S_1}|_{x=l_\mathrm{m}}\right)^{-1}\begin{bmatrix} \delta|_{l_\mathrm{m}}^{+} - \delta|_{l_\mathrm{m}}^{-} \\ \left.\frac{d\delta}{dx}\right|_{l_\mathrm{m}}^{+} - \left.\frac{d\delta}{dx}\right|_{l_\mathrm{m}}^{-} \end{bmatrix} = \left(\boldsymbol{S_1}|_{x=l_\mathrm{m}}\right)^{-1}\begin{bmatrix} 0 \\ \left.\frac{d\delta}{dx}\right|_{l_\mathrm{m}}^{+} - \left.\frac{d\delta}{dx}\right|_{l_\mathrm{m}}^{-} \end{bmatrix} \tag{72}$$

where, l_m = distance of a bend from the free end (Fig. 3) and m = 1 for Bend 1 and m = 2 for Bend 2. At a bend, the slips are continuous hence the change in slip is zero in Eq. (72) but the slip strain is not because a step change in force occurs. The change of slip strain in the Eq. (72) can be obtained from Eqs. (68) and (69) for Bend 1 and Bend 2, respectively

Similarly, the change of coefficient vectors for Zone II and Zone III can be derived as:

$$\boldsymbol{c_2^+}|_{l_\mathrm{m}} - \boldsymbol{c_2^-}|_{l_\mathrm{m}} = \left(\boldsymbol{S_2}|_{x=l_\mathrm{m}}\right)^{-1}\begin{bmatrix} 0 \\ \left.\frac{d\delta}{dx}\right|_{l_\mathrm{m}}^{+} - \left.\frac{d\delta}{dx}\right|_{l_\mathrm{m}}^{-} \end{bmatrix} \tag{73}$$

$$\boldsymbol{c_3^+}|_{l_\mathrm{m}} - \boldsymbol{c_3^-}|_{l_\mathrm{m}} = \left(\boldsymbol{S_3}|_{x=l_\mathrm{m}}\right)^{-1}\begin{bmatrix} 0 \\ \left.\frac{d\delta}{dx}\right|_{l_\mathrm{m}}^{+} - \left.\frac{d\delta}{dx}\right|_{l_\mathrm{m}}^{-} \end{bmatrix} \tag{74}$$

Application of the above components for final solution of global load-slip (Pt-Δ)

The above section describes the additional mathematical relations required to consider the effect of bends in hooked fibre. The solution is otherwise the same as the straight fibre except that the coefficient vector changes at the bends. The procedure for applying the solution to the hooked fibres is given in Fig. 8 as follows:

1) A free end slip δ_{0_i}. is imposed on the fibre.

2) The fibre embedment length L is reduced by the free end slip δ_{0_i}

3) The initial values of the coefficient vectors are defined using δ0i and the boundary condition $\frac{d\delta}{dx}$ = 0 at the free end.

4) A check is made to identify if a transition point between zones occurs before reaching the end of the fibre.

5) If a transition point is reached before the end of the fibre, the coefficient vectors in step 3 are updated to allow for the presence of multiple zones.

6) If a bend is reached the coefficient vector is further updated to allow for the step changes in force at the bend.

7) Once the coefficient vector is know, at the loaded end Δ and $\frac{d\delta}{dx}$ can be determined and from $\frac{d\delta}{dx}$the force is fibre $P_{f_{\mathrm{i}}}$ is also known.

Validation of numerical and analytical solutions

The above analytical and numerical solutions are now validated using the test results of Cunha et al. (2007) and Abdullah & Ree (2019) who conducted single fibre pull-out tests on straight and hooked fibres of identical diameter. These tests are chosen over others that are available in the literature as the identical fibre type and mechanical properties allow for a direct validation of the hinge component of the model.

Cunha et al. (2007) tested DRAMIX® RC-80/60-BN hooked steel fibres with a diameter of 0.75mm and an average yield strength of 1141 MPa. Embedment lengths of 20mm and 30 mm where considered. The concrete had a compressive strength at the time of testing of 83.4 MPa. The modulus of elasticity was calculated according to AS 3800-2018B as 39,600 MPa. The straight fibres were manufactured by using pliers to remove the hooks. The fibre geometry is shown in Fig. 9.

In Fig. 10(a) and (b) the experimental results for straight fibres from Cunha (2007) are used to calibrate the local τ/δ material properties. The calibrated interfacial bond-shear stress properties

were found τ_f = 2 MPa, τ_r =1.3 MPa, δ_1 = 0.2 mm and δ_2 = 0.4 mm. It is also worth noting that the outputs from numerical and analytical models are identical in Fig. 10a, b.

Abdallah and Ree (2019) tested hooked end fibres with a fibre diameter of 0.9 mm and an embedment length of 30 mm. Different concrete strengths were considered including 33 MPa, 54 MPa and 72 MPa. The concrete elastic modulus for these concretes were calculated as 30,500 MPa, 35,500 MPa, and 38,500 MPa, respectively.

In Fig. 10(c),(d) and (e) the experimental results for straight fibres from Abdallah & Ree (2019) where then used to calibrate the local τ/δ material properties. For the 33 MPa concrete the calibrated interfacial bond parameters are τ_f = 0.7 MPa, τ_r = 0.3 MPa. For the 54 MPa concrete these parameters are τ_f = 0.9 MPa, τ_r = 0.4 MPa. For the 72 MPa concrete these parameters are τ_f = 1.3 MPa, τ_r = 0.6 MPa. For all concrete strengths δ_1=0.05 mm and δ_2=1.5 mm.

The bond-shear properties of fibres are unique to each combination of concrete and fibre type. The calibrated interfacial bond-shear properties are then used to simulate the hooked end fibres. It was however found that the frictional property (τ_r) needed to be recalibrated for hooked fibres as the hooks does not straighten completely inducing additional friction. The need for this adjustment is also seen in other models as well for example Soetens et al. (2013). The τ_r was then recalibrated using the hooked fibre test results. These were found as 0.69 MPa, 0.89 MPa, and 1.29 MPa for the 33 MPa, 54 MPa, and 72 MPa cases respectively.

The ultimate pull-out load was then compared to calibrate the additional frictional property (μ) of hooked fibre. The μ properties from Fig. 11(a) (20mm embedment length in Cunha 2007), and Fig. 11© (30mm embedded fibre in 33 MPa concrete for Abdallah and Ree, 2019's), were thus determined as 0.01, and 0.2, respectively.

These properties are now used to simulate the hooked end fibres in Fig. 11. This demonstrates a close correlation between the experimental results and the analytical model.

Parametric study

Having validated the model above, it can now be used as the basis for a parametric study. Before presenting numerical results let us first consider the generic influence of parameters on the P_f/Δ relationship shown in Fig. 12(a) where the response of a hooked fibre is compared to that of a straight fibre.

The complete pull-out response of the straight fibre in Fig. 12(a) can be described by considering the distributions of interfacial shear stress in Fig. 12(b) as follows:

Region 0-1: the force is resisted entirely by the interfacial shear stresses which are limited to the linear ascending region (zone I in Fig. 12(c)).

Region 1-1': the slip at the free-end exceeds δ_1 in Fig. 6(a) such that the distribution of shear stress is as shown in Fig. 12(c) and contains zone I and II, only II, or zone II and III. Here these scenarios are not differentiated because the small fibre length makes graphical identification of the transition point difficult.

Region 1'-ultimate fibre pull-out: the slip at the free end exceed δ_2 in Fig. 6(a) such that only frictional resistance remains and hence only zone III applied in Fig. 12 (d).

Now let us consider the additional forces with arise due to the plastic hinge formation the frictional contribution arising from the bend.

Region 0-1: as with the straight fibre, the interfacial bond is restricted to Zone I and the hook plastic hinge and frictional contributions are small but increase with slip.

564 Region 1-1': the hook plastic hinge and frictional contributions continue to increase with slip
565 while the interfacial bond contribution decreases as zones I-III are introduced.

566 Region 1'-2: the interfacial shear stress contribution arises only due to friction (Zone III), while
567 the contribution of the plastic hinge continues to increase with slip, reaching its maximum
568 contribution at point 2. Similarly, the frictional force $F_{\mu 2}$ (occurring at the second hook)
569 continues to increase until point 2 while the frictional force $F_{\mu 1}$ (occurring at the first hook)
570 decreases. The reduction in force at $F_{\mu 1}$ occurs as a result of the reduction in interfacial shear
571 stresses along the fibre between the free end and hook 1 in Fig. 3. Conversely, the force $F_{\mu 2}$
572 continues to increase because at the location of the second hook the overall frictional force
573 increases despite the reduction in interfacial bond stresses because both the interfacial bond
574 force and the plastic hinge force P_{PH1} contribute to friction.

575 Region 2-3: All interfacial shear stresses arise only due to friction and all plastic hinge forces
576 are fully developed.

577 Region 3-4: the free-end of the fibre begins to slip beyond the first bend such that the plastic
578 hinge force at bend 1 is reduced and falls to zero at point 4.

579 Region 4-5: the free-end of the fibre has slipped past the first bend such that only a single hook
580 is still embedded in the concrete. The behaviour of the remaining hook and the interfacial shear
581 is identical to region 3-4.

582 Region 5-6: the free-end of the fibre begins to slip beyond the second bend such that the plastic
583 hinge force at bend 2 is reduced and falls to zero at point 6.

584 Region 6-ultimate fibre pull-out: the behaviour is identical to a straight fibre with only friction
585 (zone III).

586 Having identified the influence of the number and location of the hooks on the generic shape
587 of the P_f-Δ relationship above, let us now consider a parametric study with the following sets
588 of variations: (a) number of hooks, (b) fibre diameter, (c) fibre embedment length, (d) hook
589 position along the fibre length, (e) distance between the bends, (f) bend angle in a hook. For
590 the purpose of this study a steel fibre of geometry as shown in Fig. 9 is considered as the
591 baseline and the local τ-δ properties and μ are taken as those identified in the validation. The
592 remaining parametric variations are described in Table 1.

593 The parametric study considering a variation in the number of hooks is shown in Fig. 13(a), in
594 which it is observed that as the number of hooks increases the force generated at a given slip
595 also increases due to the additional plastic hinge and frictional forces. This increase in force
596 with an increase in hook number will be limited by the strength of the fibre such that it is not
597 possible to continue to add additional hooks indefinitely. The enhancement of pull-out load
598 due to addition of bends in hooked fibre was also experimentally proven by Abdallah and Ree
599 (2019).

600 The influence of fibre diameter is shown in Fig. 13(b), which is plotted in terms of fibre stress
601 rather than fibre force as it allows for the comparison of fibre efficiency. When considering the
602 influence of diameter, it is important to consider that the interfacial bond stresses vary
603 proportionally with fibre diameter, but the plastic hinge contribution varies proportionally with
604 the diameter squared.

605 The influence of fibre embedment length is shown in Fig. 13(c) in which it can be seen that
606 pull-out loads and particularly energies are significantly impacted by embedment length. The
607 reason for this reduction is the drop in load developed by interfacial shear, which is directly
608 proportional to the embedded length. Robins et al. (2002) investigated the influence of straight
609 fibre embedment lengths (5, 10, 15, and 20mm) on the pull-out load and slip response. There

610 was a significant difference of ultimate pull-out load between 5mm, and 10mm embedment
611 length, but this difference was insignificant for 10, 15, and 20mm embedment length.

612 The effect of hook position along the fibre length is shown in Fig. 13(d). It is observed that
613 while the maximum force is independent of the position of the hook, the post peak behaviour
614 is highly dependent on hook location. This is because the slip to cause pull-out of the hook
615 depends on hook location and can be increased by shifting the hook closer to the loaded end.
616 A similar phenomena is observed in Fig. 12(e) which shows the influence of the distance
617 between bends. In this case it is observed that by increasing the distance between hooks the
618 slip to cause at which the second bend becomes inactive is increased and therefore so too is
619 pull-out energy.

620 The significance of the angle of the bend of the hook is shown in Fig. 13(f) where it is seen
621 that by increasing the angle of the hook the ultimate force can be significantly increased. This
622 occurs because both the plastic hinge force and the frictional force are directly related to the
623 bend angle (θ). From Eq. 9 F_{PH} for $\theta = 45^0$, and 60^0 is 1.22 and 1.73 times higher than F_{PH} for
624 $\theta = 30^0$, there is however a limit to which the angle of the fibre can be increased before which
625 fibre rupture will occur.

626 **Conclusion**

627 The ductility of fibre-reinforced concrete depends on the matrix (concrete) and fibres where
628 the type and fraction of fibres play a significant role. Availability of a reliable model that can
629 credibly predict the behaviours of fibre-reinforced concrete has the benefit of avoiding
630 numerous trial experiments involving time and cost to optimise the mix-design. To address this
631 issue, many researchers attempted to develop analytical and numerical models where
632 simulating the pull-out behaviour of a single straight or hooked fibre is the key problem. In
633 earlier studies, the resistance provided by the bents of a hooked fibre is only considered after

634 the complete interfacial debonding over its entire embedded length to simplify the derivation
635 of the model. As fibres move/slip during debonding phase, the resistance exerted near the bends
636 due to fibre straightening in the form of hinge should be accommodated at these localised
637 sections before complete debonding. Hence, it is a need for development of a realistic
638 prediction model that can accommodate the transfer of interfacial bond stresses and the fibre
639 straightening bending forces at hinges throughout the entire pull-out process. It is also
640 preferable to derive an analytical model, if possible, as it can be conveniently used without any
641 concern related to computational issues commonly faced by a numerical model. Such an
642 attempt is made in this study.

643 The development of the proposed analytical model is an extension of a previous approach
644 developed for the bond behaviour of plates externally bonded to brittle substrates with anchors.
645 The bends replace the anchors of the previous model where the force at the bends is a function
646 of the friction at the bend as well as the hinges that form as the fibre is straightened. The
647 solution utilises an innovative matrix-based approach to avoid defining an excessive number
648 of solution cases that arise due to the trilinear bond stress-slip relationship and the bends in the
649 fibre. The model allows for the gradual increase and then decrease in the forces at the bend
650 without using smoothing polynomials. Comparison to experimental results from Cunha (2007)
651 validate the analysis.

652 The effects of hooks, its size and position along fibre length and fibre diameter in pull-out were
653 then explored using the analytical model: The findings from this parametric study include: (1)
654 an increase in the number of hooks along the fibre length improves the pull-out resistance. (2)
655 The effect of the position of hooks is significant whereas the size of hook has less effect in
656 pull-out strength. (3) Increase of bend angle increases the pull-out strength. (4) The effect of
657 fibre embedment length has a minor influence on the ultimate pull-out resistance of the hooked

fibre as most of the ultimate pull-out resistance is attributed to the hooks. Hence, the developed analytical model can be used as a simple tool to optimise the shape and size of hook fibre for improved ductility of fibre reinforced concrete materials.

Data Availability Statement

All data, models, and code generated or used during the study appear in the submitted article.

Acknowledgements

This material is based upon work supported by the Australian Research Council Discovery Project 190102650. First author acknowledges gratefully the Adelaide Scholarship International to facilitate this research work.

Notations

The following symbols are used in this paper:

A_c = effective cross-sectional area of concrete ($A_c = (E_f / E_c).A_f$);

A_e = area of the elastic region in fibre cross-section;

A_f = cross-sectional area of fibre;

A_p = area of the plastic region in fibre cross-section;

B_m = Bond force at fibre-concrete interface of infinitesimal segment *m*;

$\boldsymbol{c}_{1,2,3}$ = initial coefficient vectors;

d_f = diameter of fibre cross-section;

dx = infinitesimal length along the embedded length;

E_f = modulus of elasticity of fibre material;

E_c = modulus of elasticity of concrete;

$F_f(l_1^+)$ = fibre force immediately after bend 1;

$F_f(l_1^-)$ = fibre force immediately before bend 1;

$F_f(l_2^+)$ = fibre force immediately after bend 2;

682 $F_f(l_2^-)$ = fibre force immediately before bend 2;

683 F_{PH} = force necessitates formation of plastic hinge;

684 F_{PH1} = force necessitates formation of plastic hinge at bend 1;

685 F_{PH2} = force necessitates formation of plastic hinge at bend 2;

686 $F_{\mu 1}$ = force due to additional friction at first bend;

687 $F_{\mu 2}$ = force due to additional friction at second bend;

688 f_c = concrete compressive strength;

689 f_y = steel fibre yield strength;

690 I_f = second moment of area of the fibre section;

691 L = embedded length of the fibre;

692 L_p = fibre bonded perimeter;

693 M_y = yielding moment when extreme fibre is just started yielding;

694 M_{PH} = moment necessary to produce plastic hinge;

695 m = 1, 2, 3, …, m (infinitesimal segment number from loading end);

696 N = normal force acting normal to the inclined segment of the fibre;

697 N_1 = normal force acting at bend 1;

698 N_2 = normal force acting at bend 2;

699 P = pull-out load;

700 P_c = reaction force on concrete from support in the pull-push experiment set up;

701 P_{c_m} = concrete force at the same level of infinitesimal fibre element (m);

702 P_f = global pull-out force in fibre;

703 P_{f_m} = fibre force in the infinitesimal element m;

704 r = radius of fibre cross-section;

705 $\boldsymbol{S}_{1,2,3}$ = solution matrix for Zone I, II, and III. subscript (1,2,3) refers the zone;

706 x = position from end of embedded length;

707 y = vertical distance of a point from neutral axis in fibre cross-section;

708 y_1 = vertical distance of elastic end from neutral axis in fibre cross-section;

709 δ = local slip at any point along fibre length;

710 $\delta_{(m)}$ = local slip at m along fibre length;

711 δ_0 = local slip at fibre free end;

712 δ_1 = local slip at ultimate bond-shear stress (τ_f);

713 δ_2 = local slip when $\tau = \tau_r$;

714 ε_f = fibre strain;

715 $\varepsilon_{f(m)}$ = fibre strain at segment m;

716 ε_c = concrete strain;

717 $\varepsilon_{c(m)}$ = concrete strain at segment m;

718 θ = angle at the bend of hooked fibre (rotation angle for formation of plastic hinge);

719 μ = frictional coefficient;

720 μN = tangential frictional force;

721 μN_1 = tangential frictional force acting at bend 1;

722 μN_2 = tangential frictional force acting at bend 2;

723 τ = local bond-shear stress;

724 $\tau(x)$ = local bond-shear stress at x distance from free end;

725 $\tau_{(m)}$ = local bond-shear stress at segment m;

726 τ_f = ultimate bond-shear stress;

727 τ_r = frictional bond-shear stress at local slip of δ_2 or more;

728 χ = curvature in bending (Fig. 4);

729 χ_y = curvature at yield at extreme perimeter of fibre cross-section in bending;

730 Δ = global slip (slip at loading end);

731 $\frac{d\delta}{dx}$ = slip strain;

732 $(d\delta/dx)_m$ = slip strain at segment *m*.

733

734 **References**

735 Abdallah, S., and Rees, D. W. 2019. "Comparisons Between Pull-Out Behaviour of Various
736 Hooked-End Fibres in Normal–High Strength Concretes." *International Journal of*
737 *Concrete Structures and Materials*, 13(1), 1-15. https://doi.org/10.1186/s40069-019-
738 0337-0.

739 Akcay, B., and Ozsar, D. S. 2019. "Do polymer fibres affect the distribution of steel fibres in
740 hybrid fibre reinforced concretes." *Construction and Building Materials*, 228, 116732.
741 https://doi.org/10.1016/j.conbuildmat.2019.116732.

742 Alwan, J. M., Naaman, A. E., and Guerrero, P. 1999. "Effect of mechanical clamping on the
743 pull-out response of hooked steel fibers embedded in cementitious matrices." *Concrete*
744 *Science and Engineering*, 1(1), 15-25.

745 Barr, B. 1987. "Fracture characteristics of FRC materials in shear." *Special Publication*, 105,
746 27-54.

747 Bischoff, P. H. 2001. "Effects of shrinkage on tension stiffening and cracking in reinforced
748 concrete." *Canadian Journal of Civil Engineering*, 28(3), 363-374.
749 https://doi.org/10.1139/l00-117.

750 Boyce, W.E., Diprima, R.C., Wiley, J., and Jung, M. 2001. *Elementary differential equations*
751 *and boundary value problems*. New York:Wile, ISBN: 978-1-119-38287-4.

752 Cadoni, E., Meda, A., and Plizzari, G. A. 2009. Tensile behaviour of FRC under high strain-
753 rate. *Materials and structures*, 42(9), 1283-1294. https://doi.org/10.1617/s11527-009-
754 9527-6.

755 Casanova, P., and Rossi, P. 1997. "Can steel fibers replace transverse reinforcements in
756 reinforced concrete beams." *Materials Journal*, 94(5), 341-354.
757 https://doi.org/10.14359/9874.

758 Choi, K. K., Hong-Gun, P., and Wight, J. K. 2007. "Shear strength of steel fiber-reinforced
759 concrete beams without web reinforcement." *ACI Structural Journal*, 104(1), 12.

760 Chu, S. H., Li, L. G., and Kwan, A. K. H. 2018. "Fibre factors governing the fresh and hardened
761 properties of steel FRC." *Construction and Building Materials*, 186, 1228-1238.
762 https://doi.org/10.1016/j.conbuildmat.2018.08.047.

763 Chu, S. H., and Kwan, A. K. H. 2019. "Mixture design of self-levelling ultra-high performance
764 FRC." *Construction and Building Materials*, 228, 116761.
765 https://doi.org/10.1016/j.conbuildmat.2019.116761.

766 Cunha, V. M., Barros, J. A., and Sena-Cruz, J. M. 2010. “Pullout behavior of steel fibers in
767 self-compacting concrete.” *Journal of Materials in Civil Engineering*, 22(1), 1-9.
768 https://doi.org/10.1061/(ASCE)MT.1943-5533.0000001.

769 Eid, M. N. 2020. *Proposal of a Mix Design Method for Low Cement Fiber Reinforced*
770 *Concrete*. Doctoral dissertation, Université d'Ottawa/University of Ottawa.

771 Laranjeira, F., Aguado, A., and Molins, C. 2010a. “Predicting the pullout response of inclined
772 straight steel fibers.” *Materials and structures*, 43(6), 875-895.
773 https://doi.org/10.1617/s11527-009-9553-4.

774 Laranjeira, F., Molins, C., and Aguado, A. 2010b. “Predicting the pullout response of inclined
775 hooked steel fibers.” *Cement and concrete research*, 40(10), 1471-1487.
776 https://doi.org/10.1016/j.cemconres.2010.05.005.

777 Li, V. C., Stang, H., and Krenchel, H. 1993. “Micromechanics of crack bridging in fibre-
778 reinforced concrete.” *Materials and structures*, 26(8), 486-494.
779 https://doi.org/10.1007/BF02472808.

780 Meda, A., Minelli, F., and Plizzari, G. A. 2012. “Flexural behaviour of RC beams in fibre
781 reinforced concrete.” *Composites Part B: Engineering*, 43(8), 2930-2937.
782 https://doi.org/10.1016/j.compositesb.2012.06.003.

783 Naaman, A. E., Namur, G. G., Alwan, J. M., and Najm, H. S. 1991. “Fiber pullout and bond
784 slip. I: Analytical study.” *Journal of Structural Engineering*, 117(9), 2769-2790.
785 https://doi.org/10.1061/(ASCE)0733-9445(1991)117:9(2769).

786 Naaman, A. E., and Shah, S. P. 1975. “Bond studies on oriented and aligned steel fibres.” In
787 *RILEM Symp., Fibre Reinf Cem and Concri*, 171-178.

788 Noghabai, K. 2000. “Beams of fibrous concrete in shear and bending: experiment and model.”
789 *Journal of structural engineering*, 126(2), 243-251.
790 https://doi.org/10.1061/(ASCE)0733-9445(2000)126:2(243).

791 Olver, F. W. J., Olde Daalhuis, A. B., Lozier, D. W., Schneider, B. I., Boisvert, R. F., and
792 Clark, C. W., Miller B. R., Saunders, B. V., Cohl H. S., McClain, M. A. eds 2020. “NIST
793 Digital Library of mathematical functions.” Accessed July 16, 2021.
794 https://dlmf.nist.gov/about/news/#S1.I1.i3.

795 Robins, P., Austin, S., & Jones, P. (2002). Pull-out behaviour of hooked steel fibres. *Materials*
796 *and structures*, *35*(7), 434-442.

797 Rossi, P. 2013. “Influence of fibre geometry and matrix maturity on the mechanical
798 performance of ultra high-performance cement-based composites.” *Cement and*
799 *Concrete Composites*, 37, 246-248. https://doi.org/10.1016/j.cemconcomp.2012.08.005.

800 Schumacher, P. 2006. *Rotation capacity of self-compacting steel fiber reinforced concrete*.
801 PhD Thesis, Delft University of Technology.

802 Simões, T., Octávio, C., Valença, J., Costa, H., Dias-da-Costa, D., and Júlio, E. 2017.
803 "Influence of concrete strength and steel fibre geometry on the fibre/matrix interface."
804 *Composites Part B: Engineering*, 122, 156-164.
805 https://doi.org/10.1016/j.compositesb.2017.04.010.

806 Soetens, T., Van Gysel, A., Matthys, S., and Taerwe, L. 2013. "A semi-analytical model to
807 predict the pull-out behaviour of inclined hooked-end steel fibres." *Construction and*
808 *Building Materials*, 43, 253-265. https://doi.org/10.1016/j.conbuildmat.2013.01.034.

809 Soulioti, D. V., Barkoula, N. M., Paipetis, A., and Matikas, T. E. 2011. "Effects of fibre
810 geometry and volume fraction on the flexural behaviour of steel-fibre reinforced
811 concrete." *Strain*, 47, e535-e541. https://doi.org/10.1111/j.1475-1305.2009.00652.x.

812 Stang, H., Li, Z., and Shah, S. P. 1990. "Pullout problem: stress versus fracture mechanical
813 approach." *Journal of Engineering Mechanics*, 116(10), 2136-2150.
814 https://doi.org/10.1061/(ASCE)0733-9399(1990)116:10(2136).

815 Stang, H., and Aarre, T. 1992. "Evaluation of crack width in FRC with conventional
816 reinforcement." *Cement and Concrete Composites*, 14(2).

817 Sturm, A. B., and Visintin, P. 2019. "Local bond slip behavior of steel reinforcing bars
818 embedded in ultra high performance fibre reinforced concrete." *Structural Concrete*,
819 20(1), 108-122. https://doi.org/10.1002/suco.201700149.

820 Sturm, A. B., Visintin, P., Vaculik, J., Oehlers, D. J., Seracino, R., and Smith, S. T. 2019.
821 "Analytical approach for global load-slip behaviour of FRP plates externally bonded to
822 brittle substrates with anchors." *Composites Part B: Engineering*, 160, 177-194.
823 https://doi.org/10.1016/j.compositesb.2018.10.024.

824 Sukontasukkul, P. 2004. "Tensile behaviour of hybrid fibre-reinforced concrete." *Advances in*
825 *cement research*, 16(3), 115-122. https://doi.org/10.1680/adcr.2004.16.3.115.

826 Türkmen, Ö. S., Wijte, S. N., Vaculik, J., De Vries, B. T., and Ingham, J. M. 2020. "High-
827 speed pullout behavior of deep-mounted cfrp strips bonded with a flexible adhesive to
828 clay brick masonry." *Structures*, 28, 1153-1172.
829 https://doi.org/10.1016/j.istruc.2020.09.026.

830 Volkersen, O. 1938. "Die Nietkraftverteilung in zugbeanspruchten Nietverbindungen mit
831 konstanten Laschenquerschnitten" [The riveting force distribution in tensioned rivet
832 connections with constant tab cross-sections]. [In German.] *Luftfahrtfor schung*, 15, 41-
833 47.

834 Wille, K., and Naaman, A. E. 2012. “Pullout Behavior of High-Strength Steel Fibers Embedded
835 in Ultra-High-Performance Concrete.” *ACI Materials Journal*, 109(4).

836 Yu, R., Spiesz, P., and Brouwers, H. J. H. 2014. “Mix design and properties assessment of
837 ultra-high performance fibre reinforced concrete (UHPFRC).” *Cement and concrete*
838 *research*, 56, 29-39. https://doi.org/10.1016/j.cemconres.2013.11.002.

839 Zhang, H., and Yu, R. C. 2016. “Inclined fiber pullout from a cementitious matrix: A numerical
840 study.” *Materials*, 9(10), 800. https://doi.org/10.3390/ma9100800.

841 Zheng, Z., and Feldman, D. 1995. “Synthetic fibre-reinforced concrete.” *Progress in Polymer*
842 *Science*, 20(2), 185-210. https://doi.org/10.1016/0079-6700(94)00030-6.

843

List of Tables

847 **Table 1.** Variation of parameters

Set	ID	Ø (mm)	Θ^0	L (mm)	l_1 (mm)	l_2 (mm)	E_c (GPa)	E_y (GPa)
(a)	SF	0.75	0	30	-	-	30	200
	HF-1B		45		2	-		
	HF-2B				2	5		
(b)	Ø1	0.25	45	30	2	5		
	Ø2	0.50						
	Ø3	0.75						
(c)	E1	0.75	45	10	2	5		
	E2			20				
	E3			30				
(d)	P1	0.75	45	30	2	5		
	P2				4	7		
	P3				6	9		
(e)	S1	0.75	45	30	2	3		
	S2					5		
	S3					7		
(f)	Θ1	0.75	30	30	2	5		
	Θ2		45					
	Θ3		60					

848

List of Figures

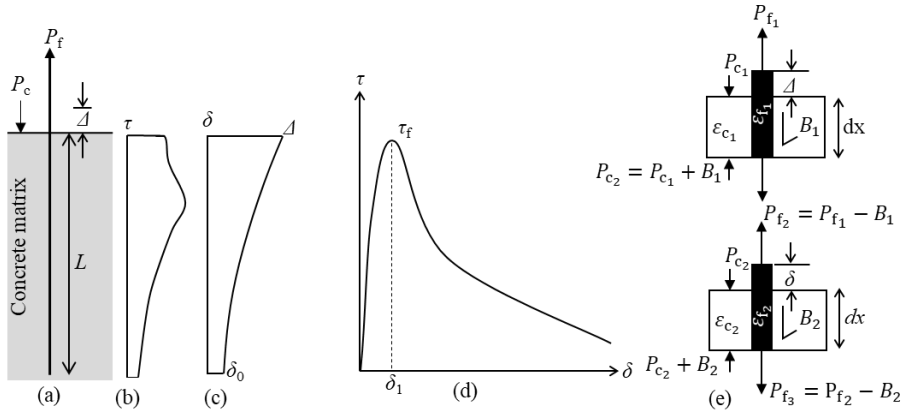

873

874 **Fig.1.** Pull-out behaviour of straight fibre: (a) straight fibre with embedded length L in
875 concrete matrix, (b) local bond/shear stress variation along the embedded length, (c) local
876 shear slip along the embedded length, (d) local bond stress - slip relationship, (e) free body
877 diagram of typical elements of infinitesimal length.

878

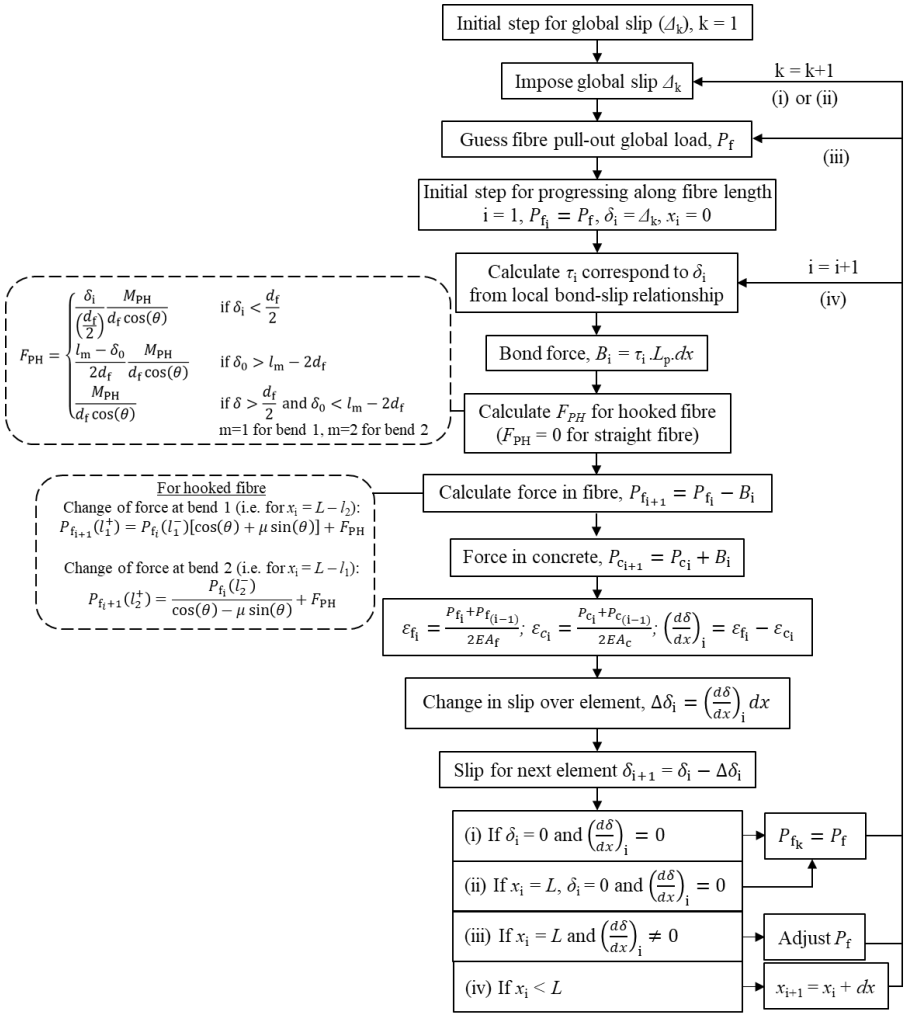

879

880 **Fig. 2.** Flow chart for numerical analysis of straight and hooked fibre pull-out load-slip.

881

882 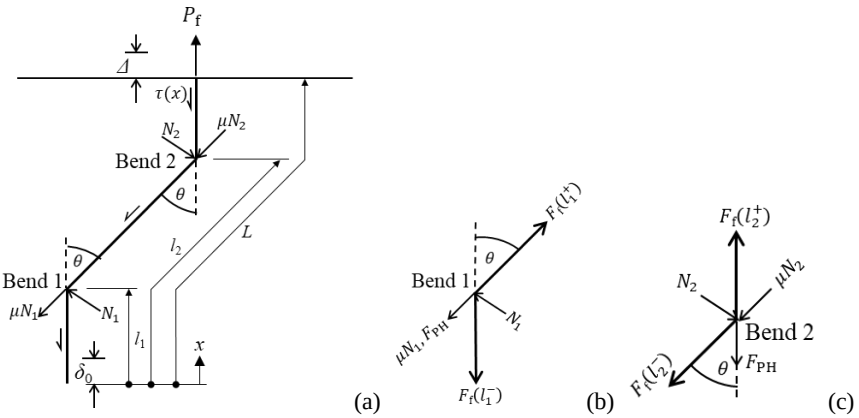

883 **Fig. 3.** (a) Forces along embedded length of a hooked fibre; (b) free body diagram of forces

884 at bend 1; (c) free body diagram of forces at bend 2.

885

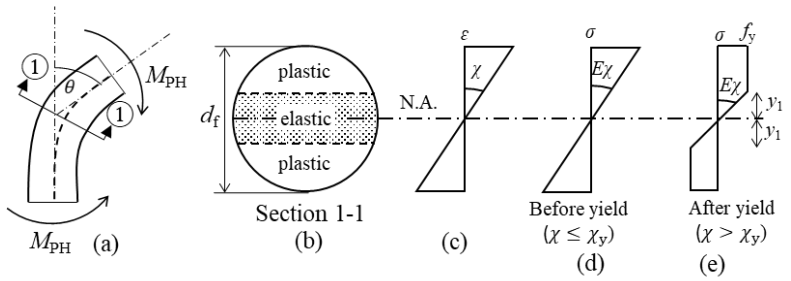

886

887 **Fig. 4.** Rotation, cross-section and strain distributions of an elastic-plastic circular fibre.

888

889 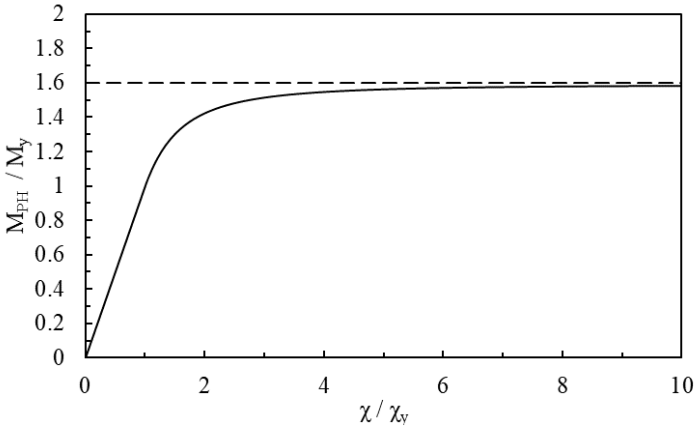

890 **Fig. 5.** Moment-curvature relationship of fibre.

891

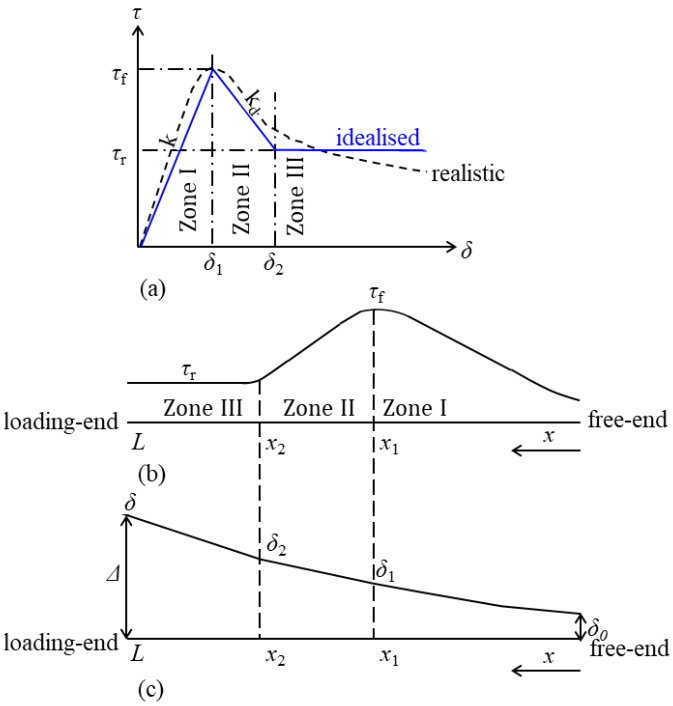

892

893 **Fig. 6.** Idealised bond stress-slip relationship and schematic variations of bond stress and slip

894 along the embedded fibre length for the three zones.

895

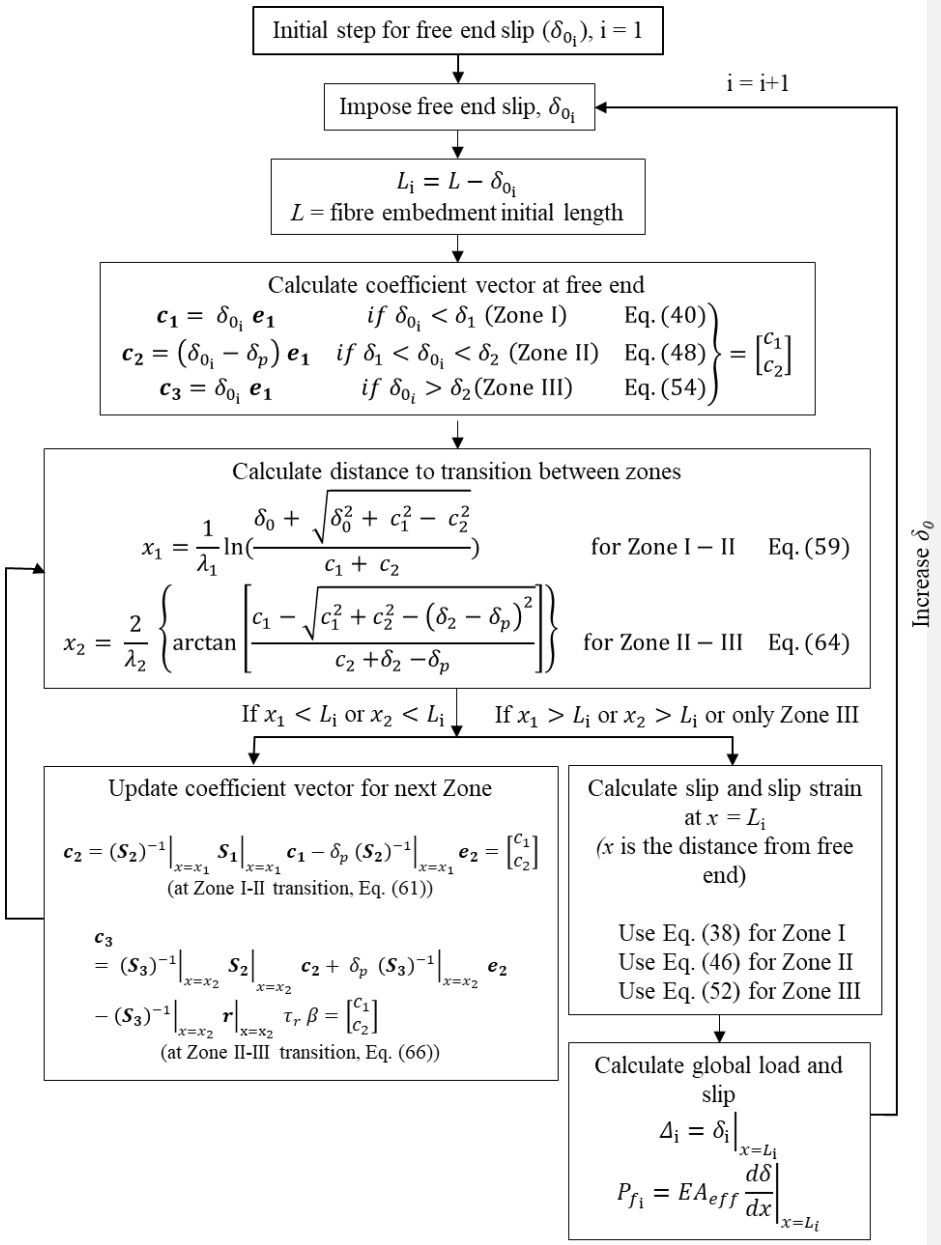

Fig. 7. Analytical solution procedure for a straight fibre.

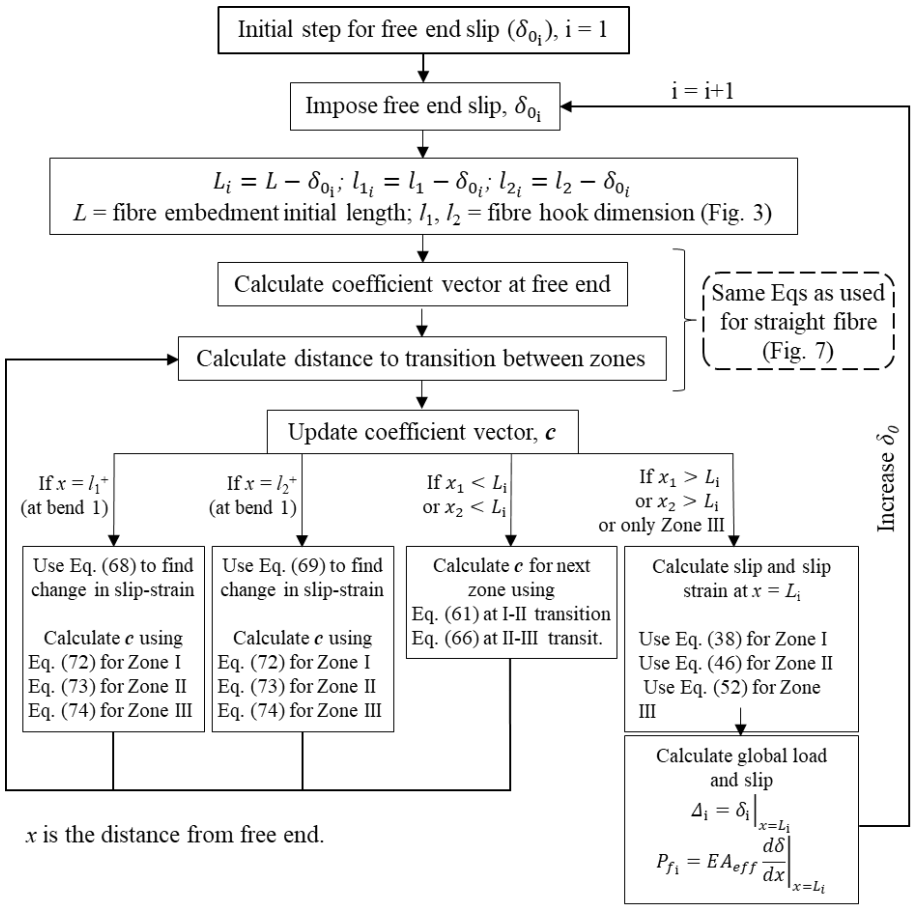

899

900 **Fig. 8.** Analytical solution for hooked fibre.

901

902

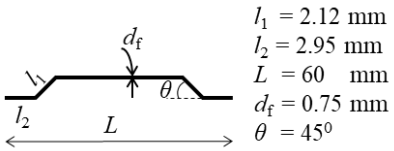

903 **Fig. 9.** Geometry of two bend-hooked fibre.

904

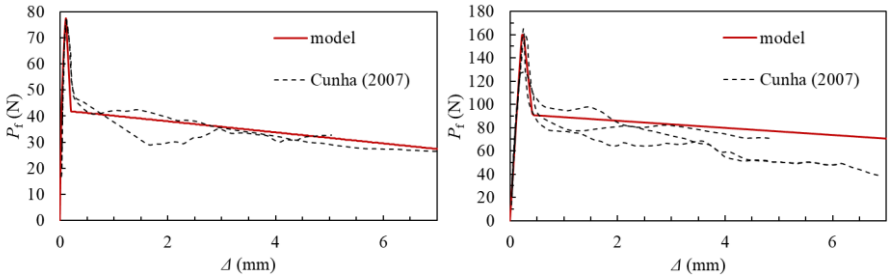

(a) (b)

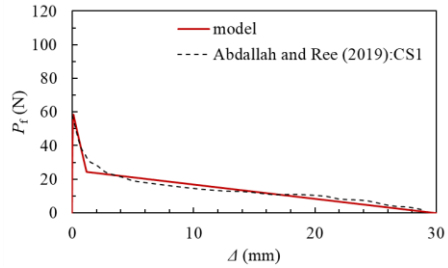

(c)

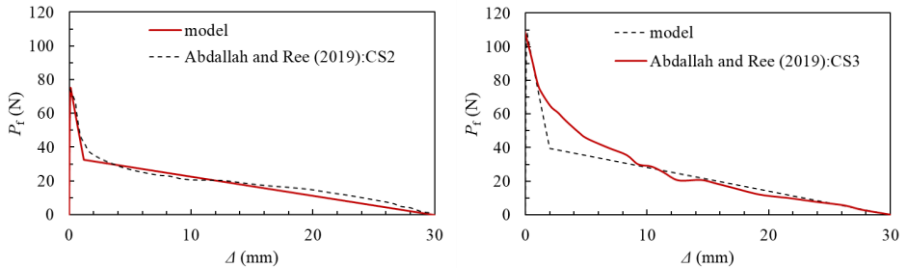

(d) (e)

Fig. 10. Straight fibre pull-out model response comparing with experimental results of Cunha (2007) for (a) 20mm, (b) 30mm embedment length, and with Abdallah and Ree (2019)'s results of 30mm fibre embedded length in (c) CS1, (d) CS2, (e) CS3

Commented [u1]: I would replace these codes with concrete strengths

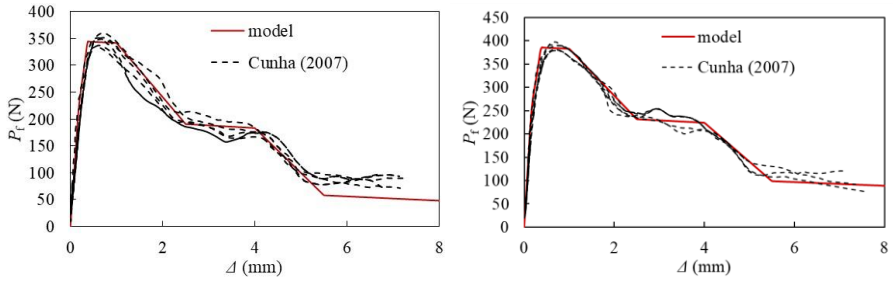

(a) (b)

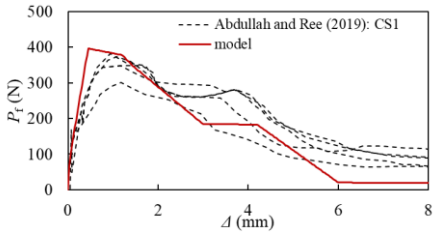

(c)

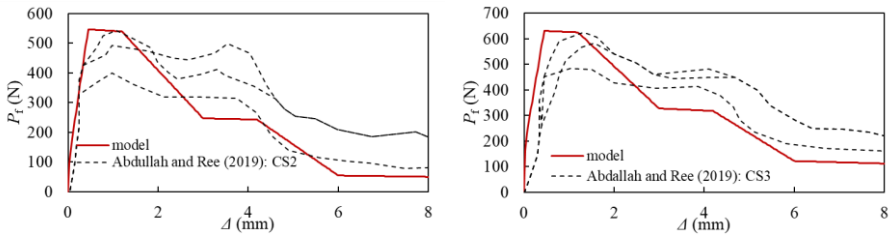

(d) (e)

Fig. 11. Hooked fibre pull-out model response comparing with experimental results of Cunha (2007) for (a) 20mm, (b) 30mm embedment length, and with Abdallah and Ree (2019)'s results of 30mm fibre embedded length in (c) CS1, (d) CS2, (e) CS3

Commented [u2]: I would replace these codes with the concrete strength

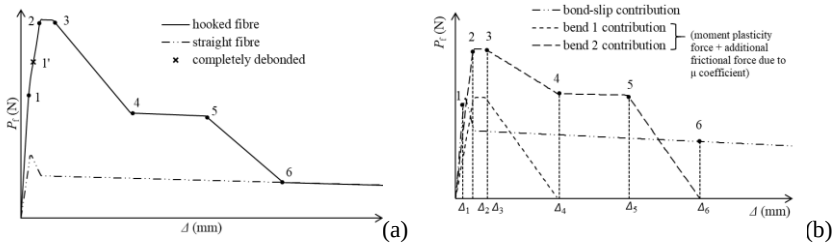

(a) (b)

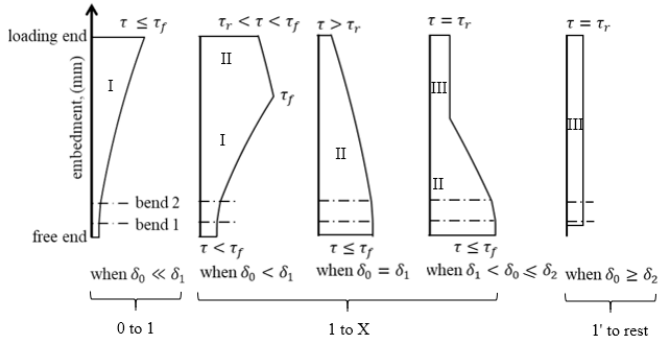

(c)

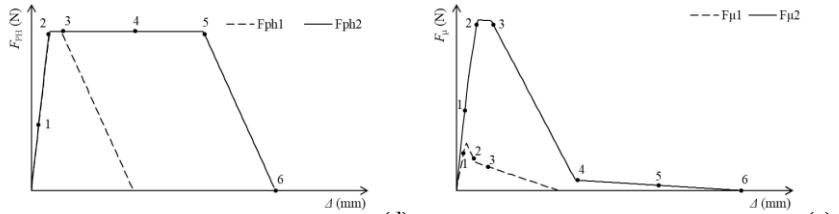

(d) (e)

Fig. 12. (a) Generic pull-out P_f-Δ behaviour of a two-bend-hooked fibre and a straight fibre embedded in concrete; (b) bend and bond-slip contribution in hooked fibre; (c) bond-shear stress at fibre-concrete interface; (d) F_{PH} for formation of plastic hinge; (e) F_μ at bend 1 and 2.

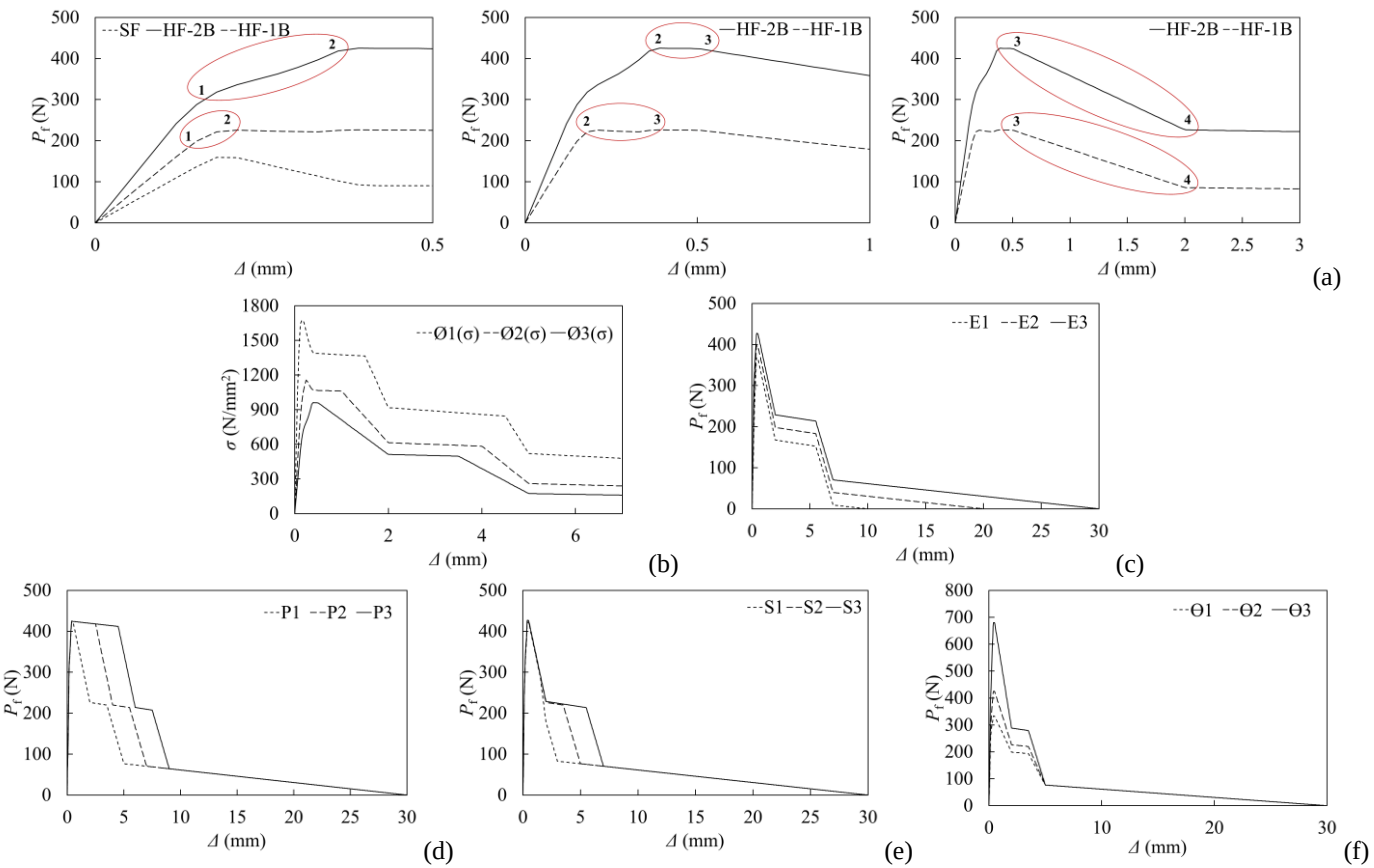

Fig. 13. Parametric study: variables are (a) straight, 1-bend & 2-bend hooked fibre, (b) fibre diameter, (c) embedment length, (d) hook position in fibre, (e) hook size, (f) bend angle.